www.elsevier.com/locate/yjtbi

Modeling Calcium Waves in an Anatomically Accurate Three-Dimensional Parotid Acinar Cell

James Sneyd, Shawn Means, Di Zhu, John Rugis, Jong Hak Won, David I. Yule

PII: S0022-5193(16)30058-3
DOI: http://dx.doi.org/10.1016/j.jtbi.2016.04.030
Reference: YJTBI8642

To appear in: *Journal of Theoretical Biology*

Received date: 26 February 2016
Revised date: 20 April 2016
Accepted date: 25 April 2016

Cite this article as: James Sneyd, Shawn Means, Di Zhu, John Rugis, Jong Hal Won and David I. Yule, Modeling Calcium Waves in an Anatomically Accurate Three-Dimensional Parotid Acinar Cell, *Journal of Theoretical Biology* http://dx.doi.org/10.1016/j.jtbi.2016.04.030

Modeling Calcium Waves in an Anatomically Accurate Three-Dimensional Parotid Acinar Cell

James Sneyd, Shawn Means, Di Zhu, John Rugis

Department of Mathematics, University of Auckland, New Zealand.

Jong Hak Won, David I. Yule

Department of Pharmacology and Physiology, University of Rochester Medical Centre, Rochester, USA

Abstract

We construct a model of calcium waves in a three-dimensional anatomically accurate parotid acinar cell, constructed from experimental data. Gradients of inositol trisphosphate receptor (IPR) density are imposed, with the IPR density being greater closer to the lumen, which has a branched structure, and inositol trisphosphate (IP_3) is produced only at the basal membrane. We show (1) that IP_3 equilibrates so quickly across the cell that it can be assumed to be spatially homogeneous; (2) spatial separation of the sites of IP_3 action and IP_3 production does not preclude the formation of stable oscillatory Ca^{2+} waves. However, these waves are not waves in the mathematical sense of a traveling wave with fixed profile. They result instead from a time delay between the Ca^{2+} rise in the apical and basal regions; (3) the ryanodine receptors serve to reinforce the Ca^{2+} wave, but are not necessary for the wave to exist; (4) a spatially-independent model is not sufficient to study saliva secretion, although a one-dimensional model might be sufficient. Our results here form the first stages of the construction of a multiscale and multicellular model of saliva secretion in an entire acinus.

Keywords: Saliva secretion, Inositol Trisphosphate Receptor, Ryanodine Receptor, Calcium oscillations, Multiscale modeling

1. Introduction

The primary role of salivary gland acinar cells is to secrete saliva, the lack of which causes a host of severe medical difficulties [1, 2]. Thus, an understanding of the mechanisms underlying saliva secretion are vital for the understanding of oral health. In every kind of salivary acinar cell, saliva secretion is controlled by the concentration of cytosolic Ca^{2+} [3]. Agonist stimulation (by, say,

*James Sneyd, j.sneyd@auckland.ac.nz

acetylcholine) leads to the release of Ca^{2+} from the endoplasmic reticulum (ER) via the production of inositol trisphosphate (IP_3), with subsequent reuptake of Ca^{2+} into the ER, leading to the emergence of periodic waves of Ca^{2+} that travel across the acinar cell. Activation of Ca^{2+}-sensitive Cl^- and K^+ channels on the apical and basal membranes leads to the transport of Cl^- through the cell and into the lumen, whereupon water follows by osmosis. Thus, the basic mechanism of saliva secretion is well understood [4, 5, 6, 7, 8, 9], and has been previously modeled in detail [10, 11, 12, 13, 14].

However, although much is understood about saliva secretion, important questions, both experimental and theoretical, remain. From the theoretical point of view, one of the most interesting questions is how the structure of the acinar cells affects the properties of the Ca^{2+} waves. Salivary acinar cells (and pancreatic acinar cells also) are polarized, with distinct apical and basal regions. Agonists such as acetylcholine or carbachol bind to their G-protein-coupled receptors on the basal region of the plasma membrane, and this is where IP_3 is produced. This IP_3 diffuses through the cells to the apical regions, which is where most of the IP_3 receptors (IPR) are situated. Ca^{2+} released from the IPR can form either localized Ca^{2+} oscillations, that are restricted to the apical regions, or can form periodic global waves that propagate from the apical region to the basal region [15, 16, 17].

Although this might seem relatively simple, there are potential problems with this hypothesis. In particular, there is evidence that Ca^{2+} feedback to the production and/or degradation of IP_3 is necessary in order for oscillations or periodic waves to exist [18]. However, the sites of IP_3 production and Ca^{2+} release are spatially separated. In other words, the mechanism that generates oscillations does not exist uniformly throughout the cell; different regions of the cell contain different parts of the mechanism, and these regions are coupled by diffusion.

Such oscillators, in which the necessary components of the oscillatory mechanism are spatially separated, have not been studied in detail, and are not well understood.

An additional question that arises is how the shape of the lumen can affect the oscillatory properties. It has been proposed [19] that there is a functional reason for the differently shaped lumen of pancreatic acinar and parotid acinar cells. In parotid acinar cells, the lumen has a highly branched structure that extends over a large part of the cell, and it has been hypothesized that this is one reason for the high speed of the intracellular Ca^{2+} wave in that cell type. Pancreatic acinar cells, on the other hand, have a smaller lumen, with less branching, which may explain the lower wave speeds seen in that cell type. The differences in wave speed are physiologically important; a high wave speed is necessary to maximize fluid secretion [13], while pancreatic acinar cells, which secrete far less fluid, can operate efficiently with lower intracellular Ca^{2+} wave speeds.

Another important question is how best a detailed three-dimensional model can be simplified. Is it possible, for example, to model saliva secretion accurately using a one-dimensional simplification, or do spatial heterogeneities in three

dimensions make this inaccurate and unsatisfactory? An answer to this question will be critical for further development of multiscale models of saliva secretion.

Here, we study these questions using a three-dimensional model of a cell that is constructed from experimental measurements. Although the model equations are solved on a quantitatively accurate domain, there remains considerable uncertainty in parameter values and some spatial distributions, and thus, overall, the model is not a quantitatively accurate representation of periodic Ca^{2+} waves in parotid acinar cells. Despite this, it still affords some quantitative insight to how the geometrical domain can affect the periodic waves. We begin by studying how the spatial separation of the oscillator components (in a realistic geometry) affects the properties of the periodic Ca^{2+} waves, and then study how the shape of the lumenal region influences the periodic waves. Finally, we consider whether a one-dimensional simplification might be sufficiently accurate to model saliva secretion (although we do not yet have a definitive answer to this question).

2. Methods

2.1. Experimental methods

Lobules of parotid tissue were fixed in ice-cold methanol for 2 mins. The tissue was incubated with antisera raised against the Na^+/K^+/ATPase and the Ca^{2+}-activated chloride channel, TMEM16A, followed by appropriate secondary antibodies. These proteins are exclusively present in the basolateral and apical membrane, respectively. The localization of the proteins was visualized by confocal microscopy using an Olympus Fluoview1000MP microscope equipped with a suite of gas and diode lasers. Images were obtained at 1024 by 1024 pixels in XY with 0.4 mm between planes in the Z dimension. The individual Z plane images were further deconvolved using a nearest neighbor algorithm using Autoquant software prior to generating a maximum intensity projection.

2.2. Geometry and Mesh Construction

Starting with the Z-stacks, we used two semi-automatic processes (one process for the cells themselves and the other process for the branching lumen) to generate a three-dimensional physical model of one cluster of parotid acinar cells. Because the Z-stacks were acquired using calibrated coordinates, it was possible to construct the model using real-world dimensions.

For the cells, we manually traced cell membrane outlines in each Z-stack image. These outlines were placed in calibrated three-dimensional space as level sets, then joined and smoothed to produce closed two-dimensional cell membrane surfaces as shown, for example, in the left-hand column of Fig. 1. For the lumen, we manually placed small boxed marker spheres on each Z-stack image wherever the lumen intersected the image plane, then collected all of these spheres in three-dimensional space as shown in the right-hand column of Fig. 1.

The cell surfaces were refined and triangulated in three-dimensional space to produce volumetric meshes suitable for Finite Element Method (FEM) simulation as shown for one cell in the left-hand column of Fig. 2. The lumen

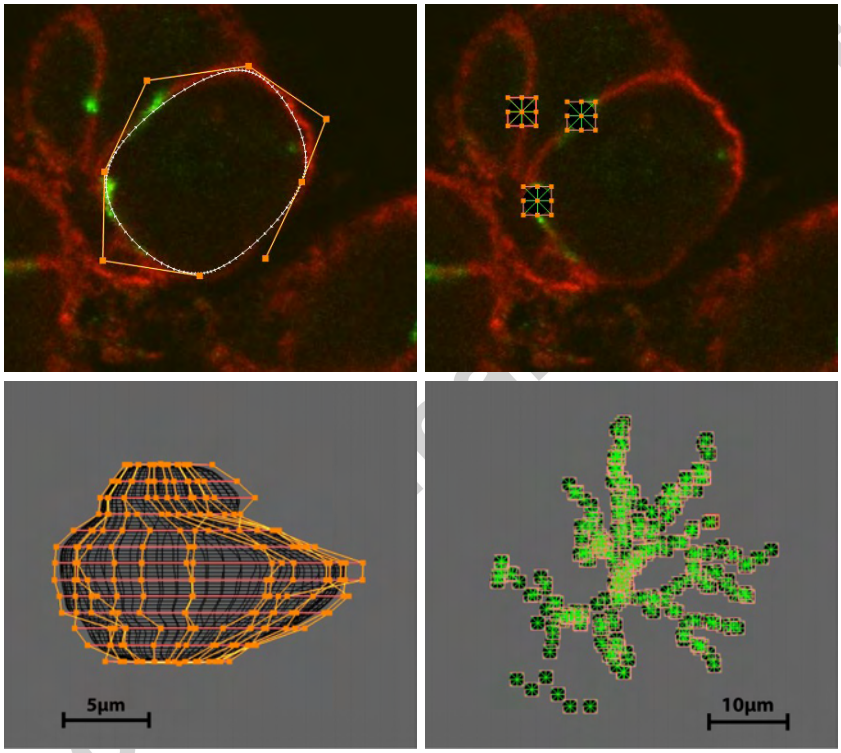

Figure 1: Top Row: tracing a cell membrane outline (left) and placing small spheres to mark the position of the lumen (right). Bottom Row: combining cell membrane level sets (left) and collecting all the lumen marker spheres (right).

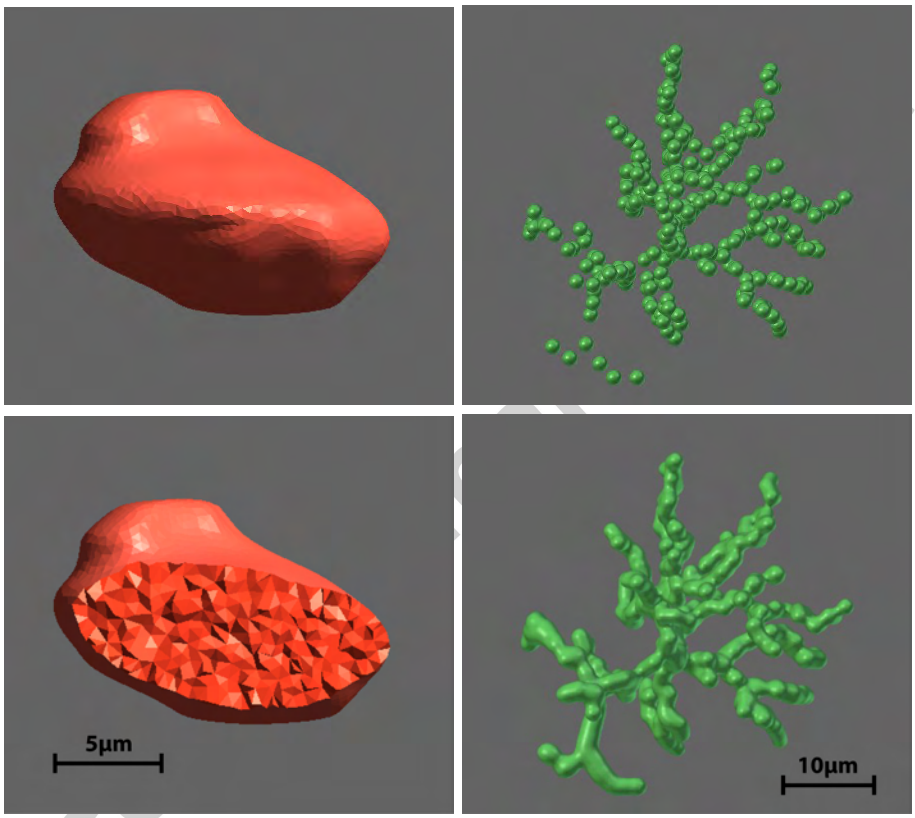

Figure 2: Top Row: refined cell membrane mesh (left) and the full collection of lumen spheres (right). Bottom Row: cut-away view of cell volumetric mesh reveals the internal tetrahedral discretization (left) and joining the lumen marker spheres together results in a finger-like branching structure (right).

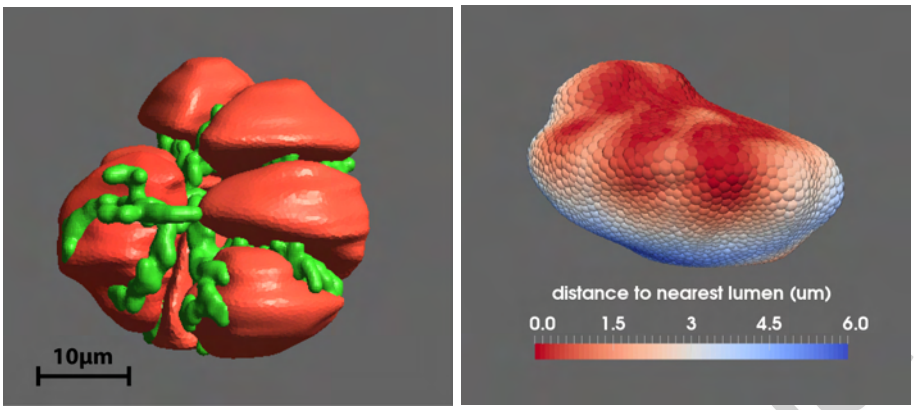

Figure 3: Left: A cluster of seven cells together with the branching lumen. Right: Nodes of one cell labeled with "distance to nearest lumen". This illustrates a lumenal imprint, i.e., the apical membrane.

marker spheres were joined together forming the parameterized tube-like structure shown in the right-hand column of Fig. 2. A complete cluster of seven parotid acinar cells with their associated lumen is shown in the left-hand side of Fig. 3. For each mesh node, the distance to the nearest lumenal membrane was calculated and assigned to each FEM node (i.e., tetrahedron vertex) as displayed for one cell in the right-hand side of Fig. 3. Similarly, the distance to the nearest basal membrane was calculated for each mesh node.

2.3. Computational methods

We implemented a custom simulation code in the C++ language, targeting high-performance cluster computing, using standard FEM methods. Within our FEM implementation, the generalized minimal residual method (GMRES) [20] from the PETSc library [21] was used as the main sparse matrix solver. A typical simulation run of two thousand time steps took twelve minutes to execute on the University of Auckland Pan cluster. For selected parameter sets we ran up to ten times longer to confirm stable Ca^{2+} oscillations. Our time step was 0.05 seconds.

To explore the model's parameter space, up to one hundred different parameter sets were run simultaneously (in parallel) on the cluster. When we extended the simulation code to include calcium diffusion in the ER, the run time increased, as expected, by a factor of approximately 1.5. The details of every simulation run were fully logged to enable tracking and reproducibility.

2.4. The mathematical model

The model of Ca^{2+} dynamics is based on the schematic diagram shown in Fig. 4. Agonist stimulation leads, via the activation of G-protein-coupled receptors, to the activation of phospholipase C (PLC) and the production of

inositol trisphosphate (IP_3), which binds to IP_3 receptors (IPR) on the ER membrane, thus releasing Ca^{2+} from the ER. The increased cytosolic [Ca^{2+}] affects the degradation of IP_3, as well as activating and inactivating the IPR, in processes that have been discussed and modeled in detail previously [12, 22].

The mathematical model is constructed by combining models of the various components. Thus, our approach is based on the idea of a Ca^{2+} "toolbox" [23], giving model equations that are similar to those in previous work [10, 24, 12, 13]. We include the fewest possible toolbox components necessary for studying the effects of spatial inhomogeneities on Ca^{2+} dynamics in acinar cells, and the model of each component is likewise taken to be of the simplest possible form that incorporates the essential behaviors of that component. This allows us to focus primarily on the effects of spatial inhomogeneities, without allowing ourselves to be sidetracked by the myriad complexities of, say, IPR models.

The model is constructed based on the following assumptions. (Here, c denotes the cytosolic [Ca^{2+}], c_e denotes the ER [Ca^{2+}], p denotes [IP_3], and h is the inactivation variable of the IPR.)

- Membrane fluxes are assumed to be negligible on the time scale of interest. Thus, we construct a closed-cell model. Although this means that our model is inaccurate over long time scales, we also know that acinar cells exhibit Ca^{2+} oscillations for a considerable time in the absence of external Ca^{2+} [25], and thus a closed-cell model is a useful way to study oscillatory behavior on shorter time scales.

- Ca^{2+} pumping from the cytosol into the ER is modeled by a Hill function, and thus

$$J_{\text{serca}} = V_s \frac{c^2}{K_s^2 + c^2}. \tag{1}$$

  For technical reasons, the model needs to include a steady-state Ca^{2+} flux out of the ER (even in the absence of IP_3). This is because our model for the SERCA pump is unidirectional, in which case the resting [Ca^{2+}] can be determined only by the balance between a non-zero SERCA flux and a non-zero leakage out of the ER. In practice, leakage out the ER is likely to be through a bidirectional SERCA pump, or through the stochastic opening of small numbers of IPR and RyRs.

  The leak flux out of the ER is modeled as

$$J_{\text{leak}} = k_{\text{leak}}(c_e - c). \tag{2}$$

  SERCA and leak fluxes are assumed to be spatially homogeneous.

- The IPR is modeled by a simple generic model of the form used by [26], [27] and [28]. Activation by Ca^{2+} is assumed to be instantaneous, while inactivation is assumed to occur on a slower time scale. Activation of the IPR by Ca^{2+} is assumed to follow a Hill function, while inactivation is assumed to follow a decreasing Hill function, with time constant τ.

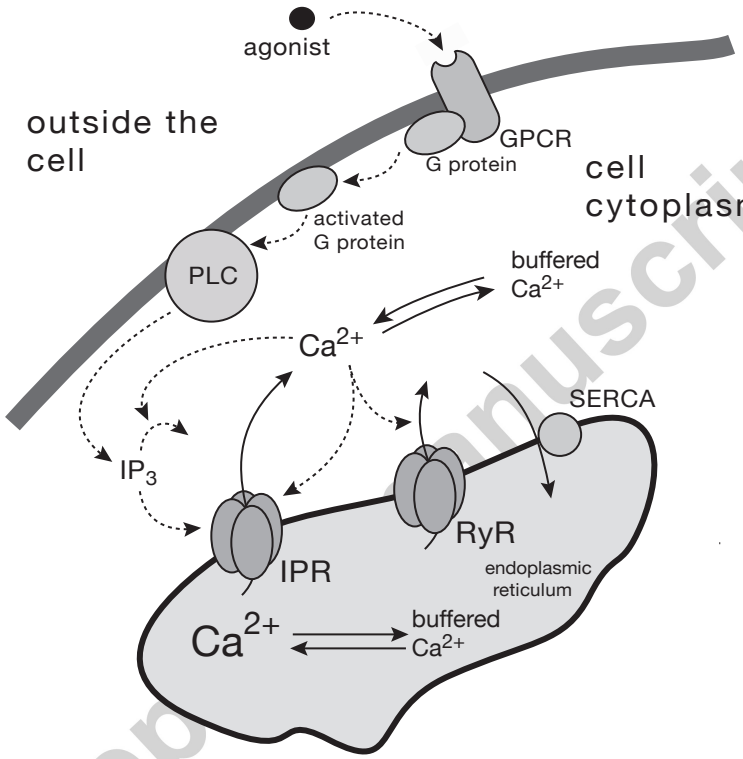

Figure 4: Schematic diagram of the Ca^{2+} fluxes and reactions included in the model. The spatial distribution of the model components is not shown. Activation of a G-protein-coupled receptor (GPCR) by agonist leads to the activation of phospholipase C (PLC) and production of inositol trisphosphate (IP_3). Although PLC itself is present through the cytoplasm, the precursor to IP_3 is membrane-bound, and thus all IP_3 production occurs at the plasma membrane. IP_3 diffuses through the cytoplasm and binds to IP_3 receptors (IPR) on the endoplasmic reticulum (ER) membrane, leading to the release of Ca^{2+} into the cytosol. Ca^{2+} can also be released from the ER by ryanodine receptors (RyR), and is pumped back into the ER by Sarcoplasmic/Endoplasmic Reticulum Ca^{2+} ATPase (SERCA) pumps.

The parameters in the Hill equations (the Hill coefficients and values for K_c, K_p and K_h) are determined from measurements of the steady-state open probability of the IPR as a function of $[Ca^{2+}]$ and $[IP_3]$. Different parameter choices are needed to model the IPR in different cell types [29]. Here, we choose parameters suitable for acinar cells, based on the single-channel measurements of [30] and the model of [31]. Activation by IP_3 is assumed to be instantaneous.

The open probability, P_o, of the IPR is thus given by

$$P_o = \frac{c^3}{K_c^3 + c^3} \frac{p^4}{K_p^4 + p^4} h, \tag{3}$$

where

$$\tau \frac{dh}{dt} = \frac{K_h^2}{K_h^2 + c^2} - h. \tag{4}$$

The flux through the IPR is then given by

$$J_{\mathrm{IPR}} = k_{\mathrm{IPR}}(\vec{x}) P_o, \tag{5}$$

where k_{IPR} models the IPR density and is a function of spatial position, $\vec{x}$.

The variable h describes the inactivation of the IPR and is introduced simply to make inactivation happen on a slower time scale to activation.

Although we know that the behavior of the IPR is considerably more complex than this simple scheme, it has also been shown that the fast activation/slow inactivation structure gives a good approximation of IPR behavior in many ways [32]. Such a simple model fails to replicate quantitatively accurate ER $[Ca^{2+}]$, and fails also to replicate the correct stochastic behavior of the IPR, but we are not concerned here with either of these things. Thus a simple model suffices.

- The ryanodine receptor (RyR) flux is modeled simply as an increasing algebraic function of $[Ca^{2+}]$ [33]. Thus

$$J_{\mathrm{RyR}} = V_{\mathrm{RyR}} \frac{c^2}{K_{\mathrm{RyR}}^2 + c^2}. \tag{6}$$

Since we wish to study the effect the RyR flux has on the Ca^{2+} oscillations, not all our simulations include an RyR flux.

- The degradation of IP_3 is assumed to be a function of $[IP_3]$ and $[Ca^{2+}]$ [28], and is spatially homogeneous. Thus,

$$\frac{\partial p}{\partial t} = D_p \nabla^2 p + V_{\mathrm{PLC}}(\vec{x}) - V_{\mathrm{deg}} \left(\frac{c^2}{K_{\mathrm{3K}}^2 + c^2} \right) p, \tag{7}$$

where p denotes $[IP_3]$. Note that V_{PLC}, the production of IP_3, is a function of spatial position, as IP_3 production occurs only at the basal membrane.

- The effects of $[Ca^{2+}]$ on fluid flow are not included, and thus our model studies the Ca^{2+} dynamics in the absence of volume changes.

- We assume that Ca^{2+} buffering is fast and linear, with non-mobile buffers, in which case all fluxes are interpreted as effective fluxes. In addition, the diffusion of Ca^{2+} is modeled by an effective diffusion coefficient.

2.4.1. Model summary

The full model equations are thus

$$\frac{\partial c}{\partial t} = D_c\nabla^2 c + J_{\rm IPR} + J_{\rm RyR} + J_{\rm leak} - J_{\rm serca}, \tag{8}$$

$$\frac{\partial c_e}{\partial t} = D_e\nabla^2 c_e + \gamma(J_{\rm serca} - J_{\rm IPR} - J_{\rm RyR} - J_{\rm leak}), \tag{9}$$

$$\frac{\partial p}{\partial t} = D_p\nabla^2 p + V_{\rm PLC}(\vec{x}) - V_{\rm deg}\left(\frac{c^2}{K_{\rm 3K}^2 + c^2}\right)p, \tag{10}$$

$$\tau\frac{dh}{dt} = \frac{K_i^2}{K_i^2 + c^2} - h, \tag{11}$$

where γ is the ratio of the cytosolic volume to the ER volume.

For simplicity, we assume that $D_c = D_e$, whereupon it follows that, letting $c_t = \gamma c + c_e$, we have

$$\frac{\partial c_t}{\partial t} = D_c\nabla^2 c_t. \tag{12}$$

In this case if we start with a constant c_t across the domain, we maintain c_t constant and spatially homogeneous for all time. This assumption of equal diffusion coefficients, which is equivalent to assuming that the cytosol and the ER have identical Ca^{2+} buffering properties, makes little quantitative difference to the model solutions. For example, setting $D_e = D_c/2$ or $2D_c$ gives solution curves which differ, at most, by 2% in amplitude and 1.3% in period. Thus we shall usually eliminate c_e by using $c_e = c_t - \gamma c$, for some constant c_t.

The parameter values are given in Table 1. It is important to note two things. Firstly, due to Ca^{2+} buffering, the diffusion coefficient of IP_3 is two orders of magnitude larger than that of Ca^{2+} (note that D_c refers to the effective diffusion coefficient of Ca^{2+}, not to its diffusion coefficient in aqueous medium). This is justified both by experiment [34] and by theoretical derivation [22]. Secondly, although $k_{\rm IPR}$ is much larger than $V_{\rm RyR}$, this does not mean that the IPR current is much larger than the RyR current. For the simple RyR model we use here, the RyR open probability is much higher than the IPR open probability. Thus, in order to have IPR and RyR Ca^{2+} fluxes of similar magnitude (which is indeed the case in our model simulations) it is necessary to make $V_{\rm RyR}$ much smaller than $k_{\rm IPR}$. An alternative approach would be to increase both $V_{\rm RyR}$ and $K_{\rm RyR}$, which would preserve the approximate magnitude of the RyR flux. However, there is no a priori reason to choose one approach over the other, so here we decided to use lower values for both $V_{\rm RyR}$ and $K_{\rm RyR}$.

γ	5.4	K_p	0.5 μM
K_c	0.3 μM	K_h	0.06 μM
τ	0.5 s	D_c	5 μm^{2}s^{-1}
V_s	0.25 μMs^{-1}	K_s	0.1 μM
k_{leak}	0.00148 s^{-1}	V_{deg}	0.1 s^{-1}
$K_{3\text{K}}$	0.4 μM	D_p	283 μm^{2}s^{-1}
V_{RyR}	0.01 μMs^{-1}	K_{RyR}	0.42 μM
d_1	0.4 μm	d_2	2 μm
$k_{\text{IPR,max}}$	10 μMs^{-1}	$k_{\text{IPR,min}}$	0 μMs^{-1}
$V_{\text{PLC,max}}$	0.016 μMs^{-1}	$V_{\text{PLC,min}}$	0 μMs^{-1}
d_3	0.8 μm	c_t	5 μM

Table 1: Model parameters for most of the model simulations. Changes in parameters for particular simulations are noted in the appropriate captions. The parameters that determine the spatial distributions are defined in Fig. 5.

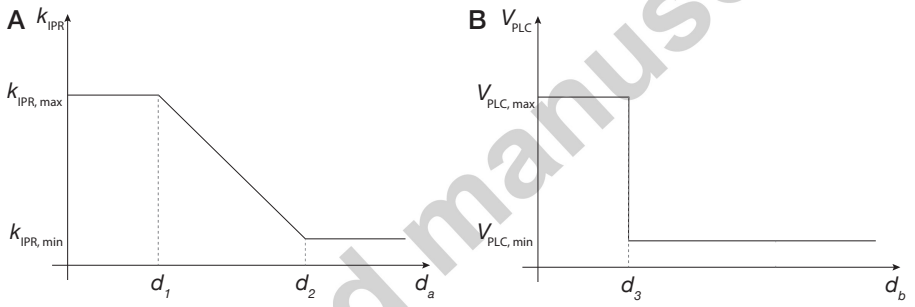

Figure 5: **A:** The IPR density, k_{IPR}, as a function of d_a, the distance to the nearest mesh point in the apical region. **B:** The rate of production of IP_3, V_{PLC}, as a function of d_b, the distance to the nearest mesh point on the basal membrane.

2.4.2. Spatial Distributions

All model parameters are spatially homogeneous, with the exception of the IPR and PLC distributions. PLC is assumed to exist only within 0.8 μm of the basal membrane, while the IPR are assumed to have a greater density in the apical regions of the cell, which have the branched structure shown in Fig. 2. Although most PLC is present through the cytoplasm, it can produce IP_3 only at the membrane, which is where the precursor to IP_3 is located, and this is most easily modelled by assuming a restricted distribution of PLC.

For each mesh point, we calculated the distance to the nearest mesh point in the apical region, and to the nearest mesh point in the basal membrane, calling these distances $d_a(\vec{x})$ and $d_b(\vec{x})$, respectively. Then, k_{IPR} is a decreasing function of d_a, while V_{PLC} is a function of d_b that is nonzero only for small values of d_b (thus restricting IP_3 production to the basal membrane).

Although it is known that IPR have a greater density in the apical region,

the exact distribution throughout the cell remains uncertain. We thus assume that k_{IPR}, as a function of d_a, takes the shape shown in Fig. 5A. The IPR density is highest near the apical region, and then descends linearly to a low constant value in the remainder of the cell. A typical three-dimensional image, color-coded by IPR density (in red) is shown in Fig. 6A.

Similarly, the PLC density takes the form shown in Fig. 5B, being thus restricted to close to the basal membrane. The distance 0.8 μm is chosen arbitrarily; because the diffusion of IP_3 is so fast that the [IP_3] is effectively spatially homogeneous, the exact value used for d_3, as long as the amount of IP_3 produced remains the same, will have no qualitative effect on the model solutions and almost no quantitative effect. A smaller value of d_3 would require a larger value of $V_{\mathrm{PLC,max}}$, so that the total amount of IP_3 produced remains constant. The PLC density is also shown in three dimensions (in blue) in Fig. 6A.

3. Results

3.1. Homogeneous Distributions

Simulations with spatially-homogeneous distributions of PLC and IPR (in which case the model collapses to a system of ODEs), serve as reference solutions that can be used as a baseline for determining how the spatial structure affects the response.

The spatially-homogeneous model behaves as expected from previous work [12, 13], as shown in Fig. 7. Oscillations occur only over a restricted range of values for V_{PLC}, and appear and disappear at Hopf bifurcations, forming a so-called *Hopf bubble*. When RyR are included in the model, the Hopf bubble increases in size as the oscillations are larger, and occur for a wider range of values of V_{PLC}. This is consistent with experimental results (from pancreatic acinar cells only) that suggest that RyR are not necessary for oscillations to exist, but only increase the size of the IPR-generated oscillations [15].

3.2. Oscillations in three dimensions

In three dimensions, with PLC making IP_3 only on the basal membrane, and with a higher density of IPR in the apical region, oscillations still occur, even though the site of IP_3 production is spatially separated from the site of Ca^{2+} release, and coupled only by the diffusion of Ca^{2+} and IP_3. This is illustrated in Fig. 8. In these simulations, RyR have been omitted from the model so that the properties of the IPR may be studied in isolation. [Ca^{2+}] in the apical region shows oscillations similar in shape and period to the oscillations in the spatially homogeneous model. However, these oscillations do not occur homogeneously through the cell, as their amplitude decreases with distance from the apical region. In the basal region, the oscillations have a very small amplitude.

Such spatially structured oscillatory solutions are typical of all solutions we obtained from the negative feedback model, for a wide range of parameters, all in the absence of RyR. That is, in this version of the model it is difficult

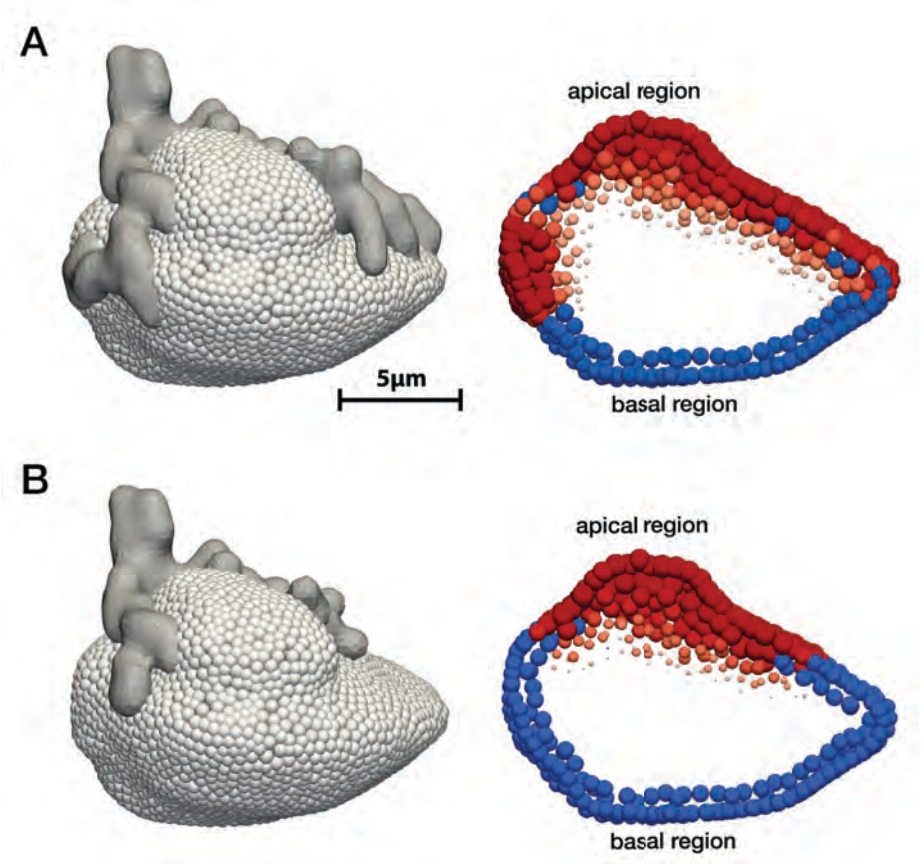

Figure 6: **A:** A three-dimensional cell and associated lumen, at full size. The right panel shows a cutaway slice view of the IPR spatial distribution (in red) and the PLC distribution (in blue). Note how the IPR distribution does not have a sharp cutoff, but decreases gradually with distance from the lumen, while the PLC distribution has a sharp cutoff, being restricted to the close proximity of the basal membrane. Note that, from the parameter values given in Table 1, the IPR cannot be more than 2 μm from the apical membrane. Similarly, the PLC cannot be more than 0.8 μm from the basal membrane. **B:** The same as the top row, except that here the lumen has been decreased in size to 60% of normal. The reduction in size was done arbitrarily, and was not based on experimental measurements. The parameter values are the same as for the top row, although now, since the lumen is smaller, the spatial distributions have changed. This smaller lumen is used for computations later in the paper.

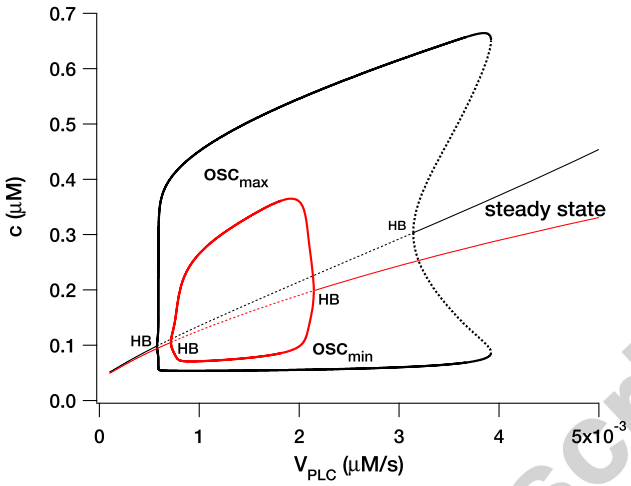

Figure 7: Bifurcation diagram of the model in the absence of diffusion. The black curves are for the model with RyR, the red curves are for the model with no RyR; $\mathrm{osc}_{\max}$ and $\mathrm{osc}_{\min}$ denote, respectively, the maximum and minimum of an oscillation over one period. Dotted lines denote unstable steady state and periodic orbits. Each version of the model has a "Hopf bubble", i.e., a branch of periodic orbits that begins and ends at a Hopf bifurcation (HB), but the Hopf bubble for the model with RyR exists for a larger range of values of V_{PLC}.

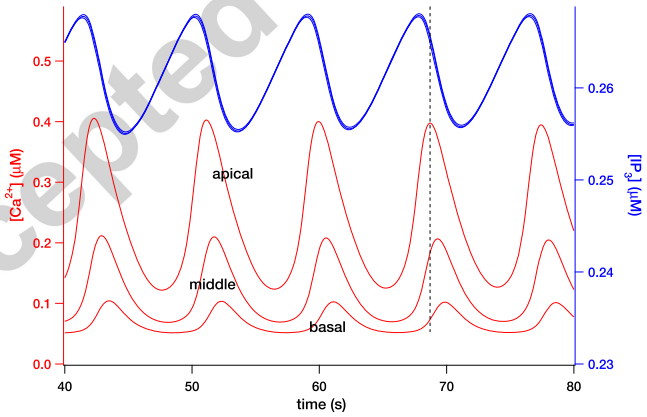

Figure 8: Solutions of the three-dimensional model (using the parameter values of Table 1), with no RyR (i.e., $V_{\mathrm{RyR}} = 0$). The graph shows three representative traces from fixed points in the cell (one apical, one basal, and one between). $[Ca^{2+}]$ is plotted in red against the left axis, while $[IP_3]$ plotted in blue against the right axis. The three curves of $[Ca^{2+}]$ from the three different regions are clearly distinct, but the three $[IP_3]$ curves lie right on top of one another. The vertical dotted line is for reference only, for better comparison of the relative timing of the peaks.

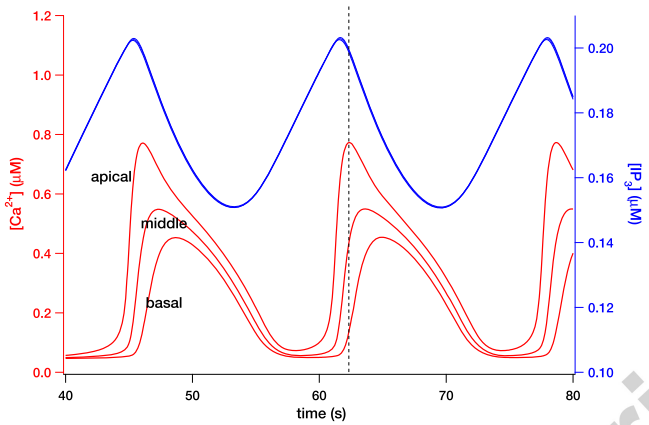

Figure 9: Solutions of the three-dimensional model. The parameter values determining the spatial distribution of IPR and PLC are the same as in Fig. 8, but with $V_{\mathrm{PLC,max}} = 0.03\ \mu\mathrm{Ms}^{-1}$. Here, as opposed to the simulations in Fig. 8, RyR are included by setting $V_{\mathrm{RyR}} = 0.01\ \mu\mathrm{Ms}^{-1}$ throughout the cell. The graph shows three representative traces from fixed points in the cell (one apical, one basal, and one between). $[\mathrm{Ca}^{2+}]$ is plotted in red against the left axis, while $[\mathrm{IP}_3]$ plotted in blue against the right axis. The vertical dotted line is for reference only, for better comparison of the relative timing of the peaks.

(and perhaps impossible) to obtain a whole-cell Ca^{2+} oscillation with the same amplitude in both basal and apical regions. This is not surprising, given the gradient of IPR density through the cell, and the absence of IPR close to the basal membrane.

3.3. The effect of RyR

In the presence of RyR the model simulations show qualitatively similar behavior, although now there is much less difference in the amplitude of the basal and apical oscillations, as Ca^{2+} release through the RyR, which are distributed throughout the cell, reinforces the release through the IPR. Typical simulations are shown in Fig. 9.

In the spatially homogeneous model we can summarize the effect of RyR in a two-parameter bifurcation diagram, using V_{PLC} and k_{IPR} as the two parameters. We can also use brute force to construct a very crude version of this diagram for the three-dimensional model. The results are shown in Fig. 10. We see that, in the spatially homogeneous model, for every constant value of k_{IPR}, addition of RyR to the model extends the range of values of V_{PLC} that give oscillations, and that as k_{IPR} increases, this range of V_{PLC} values moves to the left and gets smaller (Fig. 10A).

The same qualitative behavior is seen in the three-dimensional model (Fig. 10B). Although the exact values are different for the three-dimensional model, for every fixed value of $k_{\mathrm{IPR,max}}$, addition of RyR extends the range of $V_{\mathrm{PLC,max}}$ values for which oscillations occur. Furthermore, as $k_{\mathrm{IPR,max}}$ increases, this

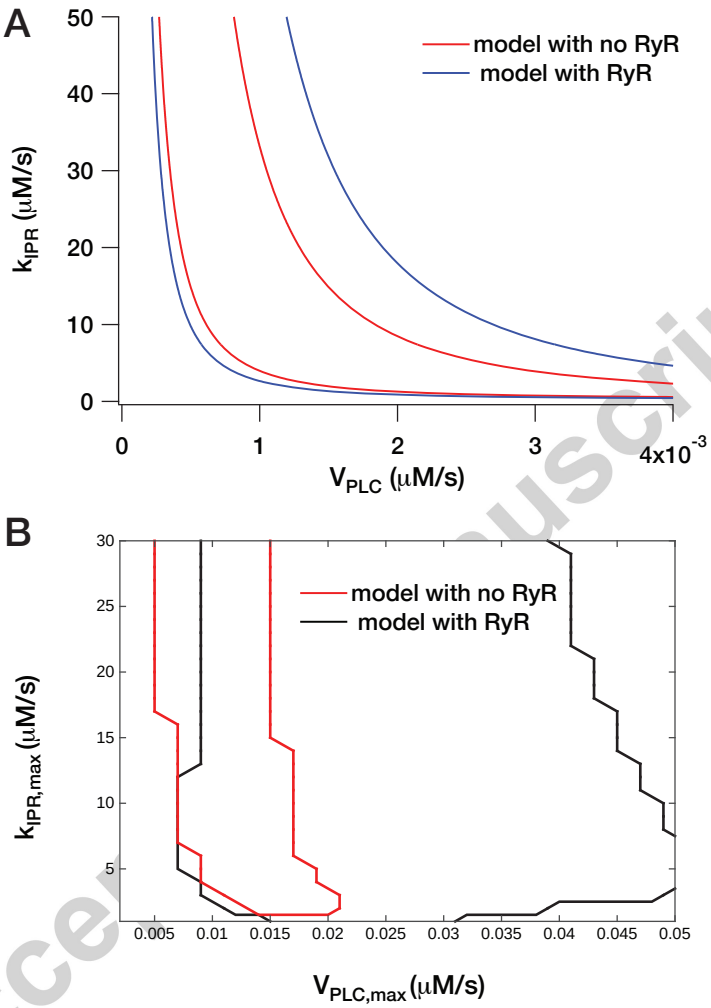

Figure 10: **A:** Two-parameter bifurcation diagram of the spatially homogeneous model. The red lines are for the model with no RyR, the blue lines are for the model with RyR. Oscillations occur only in the region between the red lines (or, in the presence of RyR, only between the blue lines). As the IPR density increases, oscillations occur for smaller values of agonist stimulation (i.e., for smaller values of V_{PLC}). **B:** The analogous two-parameter "bifurcation diagram" for the three-dimensional model. As in panel A, oscillations occur only between the red lines (in the absence of RyR) or only between the black lines (in the presence of RyR). Here, it would be difficult to generate a smooth two-parameter bifurcation diagram, and so this was computed by brute force, i.e., by solving the three-dimensional model for a range of values of $k_{\mathrm{IPR,max}}$ and $V_{\mathrm{PLC,max}}$, and keeping track of whether or not oscillations exist. The oscillation boundaries are thus only approximate.

range of $V_{\mathrm{PLC,max}}$ values moves to the left and gets smaller. Despite the crudeness of the three-dimensional "bifurcation diagram", the qualitative trends are still clear. The need for different values of $V_{\mathrm{PLC,max}}$ in the spatially homogeneous and three-dimensional models can be seen immediately once it is realized that, in both models, the $[IP_3]$ across the cell must be the same if one wishes to compare oscillations. In the spatially homogeneous model a low rate of IP_3 production is sufficient to produce enough IP_3 to generate oscillations, as this IP_3 is effectively being produced at all points of the cell. However, in three dimensions a higher rate of IP_3 production is required at the boundary in order to raise $[IP_3]$ across the cell to levels sufficient to generate oscillations.

3.4. Are the solutions in the apical region spatially heterogeneous?

In our overall goal to construct and use a multiscale model of saliva secretion over an entire parotid gland, we seek ways in which the computations may be simplified without undue loss of accuracy. We thus seek to understand how well the three-dimensional computations may be approximated by simpler computations, either in one dimension, or spatially homogeneous.

Firstly, we note that a spatially homogeneous model must, a priori, be unsatisfactory, as it cannot reproduce the large difference in $[Ca^{2+}]$ amplitude between the apical and basal regions. Since these are precisely the regions in which it is most important to calculate $[Ca^{2+}]$ accurately (as these are the regions where $[Ca^{2+}]$ controls the Ca^{2+}-dependent K^+ and Cl^- channels), we conclude immediately that a spatially homogeneous model cannot be used for a quantitatively accurate model of saliva secretion.

Secondly, we ask whether or not a one-dimensional model would be sufficient. To go some way towards answering this question, we plot $[Ca^{2+}]$ at each node close to the lumen, and at each node furthest from the lumen (the maximum distance of any node from the lumen was just less than 6 μm). For the solutions furthest from the lumen, i.e., where there are no IPR, the solutions at the nodes are very similar, in either the absence (Fig. 11A) or presence (Fig. 11B) of RyR.

However, $[Ca^{2+}]$ close to the lumen shows greater variability. Although the frequency is the same at each node (as indeed we know it must be), in the absence of RyR, the amplitude varies by approximately 13% of the maximum value. The presence of RyR decreases this variability somewhat, with a change in amplitude of only approximately 10%.

Nodes at intermediate points (say, at a distance of 2-2.1 μm from the lumen) show much greater variability (computations not shown). In the absence of RyR the amplitudes vary by over 50%, while in the presence of RyR, the amplitudes vary by over 32%. However, these intermediate Ca^{2+} concentrations are not directly controlling ion channels, and so this variability will have a lesser effect on saliva secretion.

A one-dimensional model can be constructed so as to give similar amplitudes in the basal and apical regions (computations not shown), but cannot give a variable amplitude at a fixed distance from the basal end. Thus, we know a priori that a one-dimensional model cannot give the exact same saliva secretion

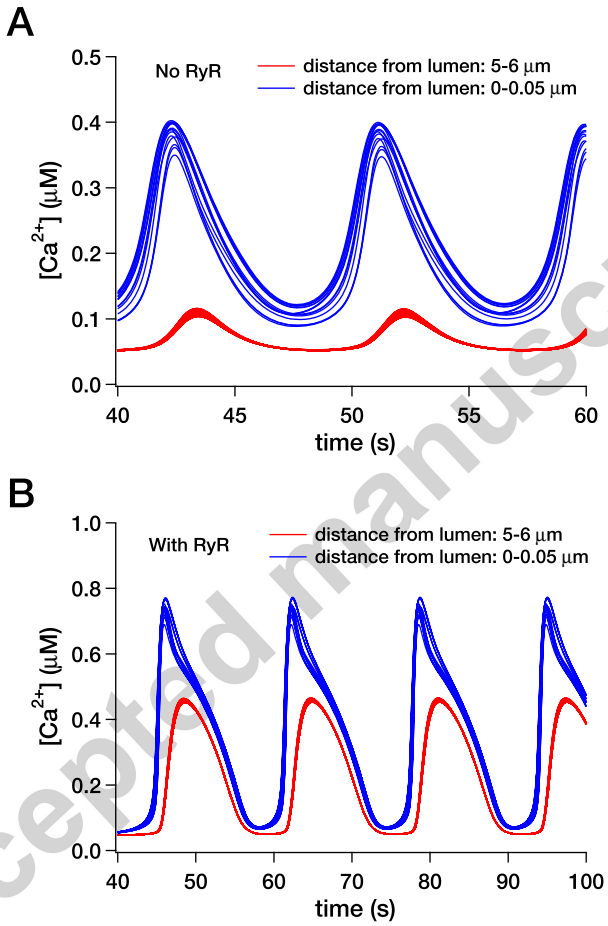

Figure 11: Heterogeneity of the three-dimensional solutions in the model without RyR (panel A) and with RyR (panel B). In each panel the blue lines are the solutions at each of the nodes close by the lumen (within 0.05 μm) while the red lines are the solutions from all the nodes at the basal end of the cell (no nodes are more than 6 μm from the closest part of the lumen). The basal solutions exhibit very little heterogeneity, but the apical solutions show much more variation, even when restricted to those nodes closest to the lumen.

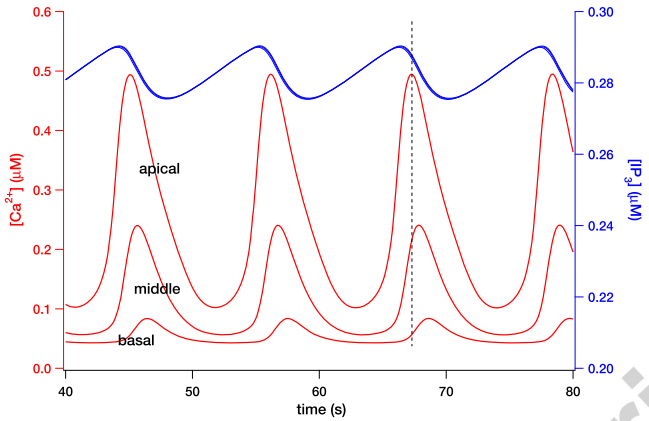

Figure 12: Solution for the smaller lumen (60% of the full-size lumen; see Fig. 6C), for $V_{\mathrm{PLC,max}} = 0.01\ \mu\mathrm{Ms}^{-1}$.

as the three-dimensional model. However, it is yet unclear how large these differences will be. To calculate these differences requires a fully detailed three-dimensional model of saliva secretion, including all the relevant apical and basal ion channels. Such a model has not yet been constructed in three dimensions (although a one-dimensional model exists [12]).

3.5. The effect of lumen size

It has been shown that the lumen of pancreatic and parotid acinar cells differ in size, and it has been hypothesized that this difference in size is related to the different function of the two acinar cell types [19]. We thus investigate how changes in lumen size affect the properties of the intracellular Ca^{2+} signaling.

The lumenal structure determined from experimental data (as shown in Fig. 3) was modified arbitrarily so that each lumenal "claw" was decreased in length by 40%. In each case, the acinar cell has a smaller lumenal surface area, and a correspondingly larger area of basal membrane. The modified lumen is shown in Fig. 6C.

The spatial distributions of IPR, PLC and RyR were left unchanged in form. Thus, PLC still exists only with 0.8 μm of the basal membrane, and IPR have a decreasing distribution that reaches zero at a distance of 2 μm from the lumenal membrane (as shown in Fig. 4, with $d_1 = 0.4$ and $d_2 = 2.0$, as in Fig. 8.) However, although the forms of the spatial distributions remain unchanged, there are important quantitative differences, as the basal and lumenal membranes are now changed in area. The new IPR and PLC distributions are shown in Fig. 6D. Thus, overall, there are more PLC and fewer IPR; the interaction between these changes makes it difficult to predict how the solutions will be affected by the change in lumen size.

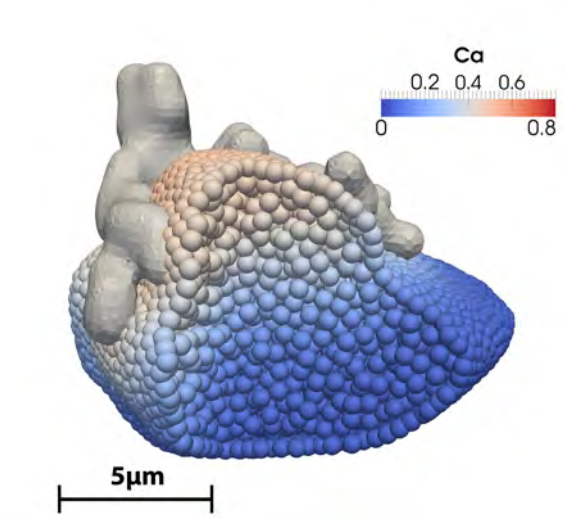

Figure 13: Simulations of the model with the smaller lumen, taken at the time point corresponding to the dashed line in Fig. 12, showing how far the oscillation extends towards the basal region.

A typical solution is shown in Fig. 12. Firstly, we note that oscillatory solutions now occur for lower values of $V_{\mathrm{PLC,max}}$, as, due to the increased size of the region where PLC exists, the previous values of $V_{\mathrm{PLC,max}}$ lead to over-production of IP_3, saturation of the receptors, and a maintained high plateau $[Ca^{2+}]$. Since this is physiologically unacceptable, such solutions must be rejected. The only remaining oscillatory solutions are those for which the apical region oscillates with physiologically reasonable amplitude, while the basal region shows only very small oscillations.

Thus, decreasing the lumen size changes the Ca^{2+} oscillations from a type that has significant amplitude oscillations in the basal region to ones where the oscillations are effectively restricted to the apical region. The extent to which the oscillation is restricted to the apical region can be seen in Fig. 13, which shows a snapshot (in cutaway view) of the intracellular $[Ca^{2+}]$, taken at the peak of the apical oscillation. Although some regions of the basal membrane show a significantly higher $[Ca^{2+}]$, most of the basal region shows very little increase in $[Ca^{2+}]$.

4. Discussion

We have constructed the first three-dimensional model of Ca^{2+} signaling in a parotid acinar cell, basing our computations on anatomically accurate reconstructions of the basal and apical membranes. Our goal was to determine how Ca^{2+} signaling is affected by the spatial structure of the parotid acinar cell,

which results in complex spatial distributions for the various components of the Ca^{2+} signaling toolkit.

Reconstruction from experimental data of the parotid cell and associated lumen shows roughly spherical cells, cradled by branches of the lumen, which has an intricate branched structure. Typically, a single acinar cell is held by a lumenal "claw" (Fig. 3) with two or three branches that extend across the acinar cell.

Our model is based on the earlier model of [12], but takes a more generic form. Thus, we omit all the complications of the IPR modal model of [31], assuming instead that the IPR steady-state open probability is a bell-shaped function of $[Ca^{2+}]$, and a sigmoidally increasing function of $[IP_3]$. In addition, we assume that inactivation of the IPR is governed by a separate inactivation variable, h. Thus, this IPR model is a slightly simplified version of the early models of [35], [26] and [28]. Our reasons for this choice are discussed later. All other model components are modeled by simple functional forms, including the RyR, which has an open probability that is an algebraic function of $[Ca^{2+}]$ [33]. Hence, no time-dependence or adaptation is included in the RyR model.

The model assumes that the IPR are located close to the apical membrane. Similarly, it assumes that PLC is situated only on the basal membrane. Thus, the sites of IP_3 production and action are spatially separated. In addition, the sites of IP_3 action have a complex spatial structure, being determined by the position of the apical membrane. We assume, for simplicity, that Ca^{2+} transport across the cell membrane can be ignored, and thus the model is of a closed cell.

Although our anatomical reconstruction was done for seven cells, for ease of presentation, all the computations shown here are from a single cell.

Our results can be summarized as follows:

1. Although IP_3 is produced only in a region close to the basal membrane, it equilibrates across the cell so quickly that it is essentially spatially homogeneous, even when $[IP_3]$ is oscillating. However, this does not necessarily mean that the diffusion equation for IP_3 can be replaced by a spatially homogeneous ordinary differential equation; this is because the degradation of IP_3 is strongly spatially dependent via its dependence on $[Ca^{2+}]$. In other words, even though IP_3 diffuses so quickly that it is effectively spatially homogeneous, Ca^{2+} does not, and thus the degradation of IP_3 cannot be assumed to be homogeneous. Hence, we cannot simply eliminate the IP_3 diffusion equation. Such elimination would require calculation of the average rate of IP_3 degradation through the cell, thus replacing the diffusion equation by an integral equation. For this reason it is simpler merely to retain the IP_3 diffusion equation.
2. Spatial separation of the sites of IP_3 production and IP_3 action does not prevent the appearance of oscillations. Although this might seem intuitively obvious, given the fact that IP_3 diffuses so quickly, that is highly misleading. In fact, since the degradation of IP_3 is Ca^{2+}-dependent, the much slower diffusion of Ca^{2+} creates a significant diffusional barrier between the apical and basal regions of the cell. This diffusional barrier

severely limits the range of parameter values for which oscillations can occur, and (for example in a large enough cell) can eliminate oscillations entirely. When oscillations exist, they invariably have a larger amplitude in the apical region than in the basal region. Indeed, for many parameter values, the Ca^{2+} can be of such small amplitude in the basal region as to be experimentally undetectable.

3. Responses in the basal region occur after the apical responses, and with a slower rise time. The basal responses of the model are slower than seen experimentally [16], but with a similar change in the rise time. Thus the intracellular Ca^{2+} waves in our model move more slowly than observed experimentally.
4. As hypothesized previously [13], the RyR function to reinforce the oscillations, in particular to increase the amplitude of the oscillations in the basal region. In general, RyR are not necessary to get oscillatory behavior, but they change the period and the amplitude significantly (compare Figs. 8 and 9).

   However, as the lumen gets smaller, the ability of the RyR to give a large basal response becomes highly restricted, and the large basal responses disappear. This result is almost certainly dependent on parameter choices, and thus it is impossible to say that the cells with a smaller lumen cannot give large basal responses under any conditions. Indeed, it is likely that this can occur for some parameter values, even if we have not found them. Nevertheless, all other things being equal, a decrease in lumen size (to 60% of normal) will eliminate oscillatory responses in the basal region, while leaving apical oscillations relatively intact, although smaller in amplitude (compare Figs. 9 and 12).

   Note that, when the lumen is decreased in size, a corresponding decrease in the rate of IP_3 production is also necessary. A smaller lumen means a larger basal membrane, which means more PLC, which means the production of more IP_3, which quickly equilibrates across the cell. As the basal membrane gets larger this saturates the cell with IP_3, preventing any oscillatory activity at all.
5. For the purposes of studying saliva secretion, a spatially-dependent model cannot be replaced by a spatially-independent model. In no case did we find spatially homogeneous Ca^{2+} oscillations across the entire cell. This is not, of course, a proof that such solutions cannot exist for our model, but we do claim them to be, if not formally impossible, at least highly unlikely. Thus, any model which uses the same $[Ca^{2+}]$ to control both the apical Cl^- channels and the basal K^+ channels must necessarily be introducing significant distortions into the results. We emphasize that, distortions or not, such models can remain highly useful, but care must be taken in any quantitative conclusions.

   It is less easy to answer the question of how well a simpler one-dimensional model would reproduce quantitatively accurate fluid transport. From Fig. 11 we see that, although $[Ca^{2+}]$ is almost exactly the same at each point of the basal membrane, $[Ca^{2+}]$ at the apical membrane still shows significant

variation. This is not unexpected, given the branched structure of the apical membrane, but the implications remain unclear. Does this amount of variation have a significant effect on fluid transport, or can the three-dimensional model be replaced by a one-dimensional version? Such a one-dimensional model will have significant inaccuracies in computing the $[Ca^{2+}]$ in the middle of the cell (we know that the variation there is much larger than that shown in Fig. 11, but we do not show the computations here), but $[Ca^{2+}]$ in the middle of the cell does not control the membrane ion channels.

We hypothesize that the variability seen in the apical responses in Fig. 11 is small enough to allow a one-dimensional model to give an accurate model of fluid flow. However, testing this hypothesis requires the extension of the three-dimensional model to include a model of fluid flow through the cell. This is a major task, and is left for future work.

In constructing our model we chose not to use a more complex, and more recent, modal model of the IPR [31], even though this model is based on single-channel measurements of IPR, and thus captures more accurately IPR properties in vivo. However, studies of these recent modal models have shown that their essential behavior can be captured in a much simpler two-variable model of the type used here. In essence, the older approaches of [35], [26] and [28], although not able to reproduce the correct single-channel behavior, still capture the correct macroscopic properties of the IPR, or at least those believed to be more directly responsible for generating Ca^{2+} oscillations. Thus, for simplicity, we chose to use a simple, generic, IPR model with the same underlying behavior.

The models for the other components of the Ca^{2+} toolkit (SERCA pumps, RyR receptors, Ca^{2+} leaks) also take simple generic forms. In addition, the model is of closed-cell type; in other words, we assume that there are no Ca^{2+} fluxes across the plasma membrane. This is a reasonable assumption, at least in the short term, as parotid acinar cells exhibit slowly-decaying oscillations in the absence of external Ca^{2+}. Thus, Ca^{2+} fluxes across the cell membrane modulate the oscillations over a slower time scale, but are not required for the oscillations to exist. Any model must therefore exhibit Ca^{2+} oscillations in the absence of Ca^{2+} influx, in which case it is simpler to omit membrane Ca^{2+} fluxes entirely.

Our model thus has the simplest possible form, which allows us to study the effects of spatial structure in the simplest possible context. However, the spatial structure of the model is also a highly simplified caricature of reality. For example, although we know that PLC is a membrane-bound protein, and thus the production of IP_3 can happen only at the membrane, we do not know that IP_3 is produced at all parts of the basal membrane. We assume this to be so in the model, but with no explicit support from data. Similarly, the model assumes that IPR are situated close to the apical membrane – which we know to be the case, at least approximately – but also assumes that there are no IPR at a distance of more than 2 μm from the apical membrane. Again, this particular number is not based on explicit data.

Because of such quantitative uncertainties, our results can be used only to

give a qualitative description of the interaction between spatial structure and Ca^{2+} signaling.

One clear example of the poor quantitative agreement of our model with experiment is the intracellular wave speed, and the delay in the basal response. In cells, the waves travel at over 20 μms^{-1} [16], considerably faster than the waves in this model, which travel at around 5 μms^{-1}. In addition, the basal response in the model begins to rise approximately 2 seconds after the apical response, which is much slower than observed. These quantitative differences are very likely the result of inaccurate IPR and RyR spatial distributions. It would be possible in principle to fit the model to data from a single cell, in order to determine the IPR and RyR distributions more accurately, but in practice there would be severe difficulties with model under-determination and thus ambiguity in the resulting parameters. For this reason we made no attempt to do this, and so have little choice but to live with quantitative inaccuracies.

The model assumes that the degradation of IP_3 is dependent on $[Ca^{2+}]$ but that the production is not. This leads to a negative feedback loop between Ca^{2+} and IP_3, a loop that has been previously studied [36, 12, 28]. Although there is evidence that the Ca^{2+} oscillations in pancreatic cells depend on simultaneous IP_3 oscillations [18], and are thus of Class II, it is not known whether Ca^{2+} affects IP_3 production or degradation. In HSY cells, there is strong evidence that Ca^{2+} affects the production of IP_3 [37], but simultaneous measurements of $[Ca^{2+}]$ and $[IP_3]$ have not been performed in parotid acinar cells. We therefore followed previous work [12] which used a model with negative feedback. There is some theoretical evidence – although no experimental confirmation – that a Class II model with positive feedback cannot give oscillations in a closed cell [38], which implies (weakly) that a model with negative feedback might be preferable, but this question is far from settled.

As yet, the three-dimensional model is not connected to a model of fluid transport through the cell, and this is something that we are currently attempting. The construction is simple in theory, as the necessary ion channels, transporters and exchangers are reasonably well characterized, but the construction is still time-consuming. It is our goal to show, by detailed comparisons between a full three-dimensional model and a one-dimensional simplification, that a three-dimensional model of the acinus is not necessary, but that fluid transport in an entire acinus of 7 or 8 acinar cells (with the accompanying branched lumen) can be well approximated by a one-dimensional branched model of the lumen coupled to one-dimensional acinar cells.

Acknowledgements

This work was funded by NIDCR grant 2R01DE019245-06A1, by the Marsden Fund of the Royal Society of New Zealand (11-UOA-148), and by a grant from New Zealand eScience Infrastructure (NeSI), funded jointly by NeSI's collaborator institutions and through the Ministry of Business, Innovation & Employment's Research Infrastructure programme.

References

[1] P. C. Fox, P. F. van der Ven, B. C. Sonies, J. M. Weiffenbach, B. J. Baum, Xerostomia: evaluation of a symptom with increasing significance, J Am Dent Assoc 110 (4) (1985) 519–25.

[2] J. E. Melvin, Saliva and dental diseases, Curr Opin Dent 1 (6) (1991) 795–801.

[3] J. E. Melvin, D. Yule, T. Shuttleworth, T. Begenisich, Regulation of fluid and electrolyte secretion in salivary gland acinar cells, Annual Review of Physiology 67 (1) (2005) 445–469.

[4] B. Nauntofte, Regulation of electrolyte and fluid secretion in salivary acinar cells, Am J Physiol 263 (6 Pt 1) (1992) G823–37.

[5] D. Cook, E. Van Lennep, R. ML, Y. JA, Secretion by the major salivary glands, in: L. Johnson (Ed.), Physiology of the Gastrointestinal Tract, 3rd Edition, Raven Press, 1994, pp. 1061–2017.

[6] J. E. Melvin, Chloride channels and salivary gland function, Crit Rev Oral Biol Med 10 (2) (1999) 199–209.

[7] R. J. Turner, H. Sugiya, Understanding salivary fluid and protein secretion, Oral Dis 8 (1) (2002) 3–11.

[8] M. C. Ashby, A. V. Tepikin, Polarized calcium and calmodulin signaling in secretory epithelia, Physiol Rev 82 (3) (2002) 701–34. doi:10.1152/physrev.00006.2002.

[9] I. S. Ambudkar, Polarization of calcium signaling and fluid secretion in salivary gland cells, Curr Med Chem 19 (34) (2012) 5774–81.

[10] J. Sneyd, K. Tsaneva-Atanasova, J. I. E. Bruce, S. V. Straub, D. R. Giovannucci, D. I. Yule, A model of calcium waves in pancreatic and parotid acinar cells, Biophys J 85 (3) (2003) 1392–405. doi:10.1016/S0006-3495(03)74572-X.

[11] E. Gin, E. J. Crampin, D. A. Brown, T. J. Shuttleworth, D. I. Yule, J. Sneyd, A mathematical model of fluid secretion from a parotid acinar cell, J Theor Biol 248 (1) (2007) 64–80.

[12] L. Palk, J. Sneyd, T. J. Shuttleworth, D. I. Yule, E. J. Crampin, A dynamic model of saliva secretion, J Theor Biol 266 (4) (2010) 625–40.

[13] L. Palk, J. Sneyd, K. Patterson, T. J. Shuttleworth, D. I. Yule, O. Maclaren, E. J. Crampin, Modelling the effects of calcium waves and oscillations on saliva secretion, J Theor Biol 305 (2012) 45–53.

[14] J. Sneyd, E. Crampin, D. Yule, Multiscale modelling of saliva secretion, Math Biosci 257 (2014) 69–79. doi:10.1016/j.mbs.2014.06.017.

[15] S. V. Straub, D. R. Giovannucci, D. I. Yule, Calcium wave propagation in pancreatic acinar cells: functional interaction of inositol 1,4,5-trisphosphate receptors, ryanodine receptors, and mitochondria, J Gen Physiol 116 (4) (2000) 547–60.

[16] D. R. Giovannucci, J. I. E. Bruce, S. V. Straub, J. Arreola, J. Sneyd, T. J. Shuttleworth, D. I. Yule, Cytosolic Ca^{2+} and Ca^{2+}-activated Cl^{-} current dynamics: insights from two functionally distinct mouse exocrine cells, J Physiol 540 (Pt 2) (2002) 469–84.

[17] A. R. Harmer, P. M. Smith, D. V. Gallacher, Local and global calcium signals and fluid and electrolyte secretion in mouse submandibular acinar cells, Am J Physiol Gastrointestinal and liver physiology 288 (1) (2005) G118–24.

[18] J. Sneyd, K. Tsaneva-Atanasova, V. Reznikov, Y. Bai, M. J. Sanderson, D. I. Yule, A method for determining the dependence of calcium oscillations on inositol trisphosphate oscillations, Proc Natl Acad Sci USA 103 (6) (2006) 1675–80. doi:10.1073/pnas.0506135103.

[19] O. Larina, P. Thorn, Ca^{2+} dynamics in salivary acinar cells: distinct morphology of the acinar lumen underlies near-synchronous global Ca^{2+} responses, J Cell Sci 118 (Pt 18) (2005) 4131–9. doi:10.1242/jcs.02533.

[20] Y. Saad, M. Schultz, GMRES: A generalized minimal residual algorithm for solving nonsymmetric linear systems, SIAM J. Sci. Stat. Comput. 7 (1986) 856–869.

[21] S. Balay, S. Abhyankar, M. F. Adams, J. Brown, P. Brune, K. Buschelman, L. Dalcin, V. Eijkhout, W. D. Gropp, D. Kaushik, M. G. Knepley, L. C. McInnes, K. Rupp, B. F. Smith, S. Zampini, H. Zhang, PETSc users manual, Tech. Rep. ANL-95/11 - Revision 3.6, Argonne National Laboratory (2015).
URL http://www.mcs.anl.gov/petsc

[22] J. Keener, J. Sneyd, Mathematical Physiology, 2nd Edition, Springer-Verlag, New York, 2008.

[23] M. J. Berridge, P. Lipp, M. D. Bootman, The versatility and universality of calcium signalling, Nat Rev Mol Cell Biol 1 (1) (2000) 11–21.

[24] K. Tsaneva-Atanasova, D. I. Yule, J. Sneyd, Calcium oscillations in a triplet of pancreatic acinar cells, Biophys J 88 (3) (2005) 1535–51. doi:10.1529/biophysj.104.047357.

[25] J. I. Bruce, T. J. Shuttleworth, D. R. Giovannucci, D. I. Yule, Phosphorylation of inositol 1,4,5-trisphosphate receptors in parotid acinar cells. a mechanism for the synergistic effects of cAMP on Ca^{2+} signaling, J Biol Chem 277 (2) (2002) 1340–8.

[26] A. Atri, J. Amundson, D. Clapham, J. Sneyd, A single-pool model for intracellular calcium oscillations and waves in the *Xenopus laevis* oocyte, Biophys J 65 (4) (1993) 1727–39. doi:10.1016/S0006-3495(93)81191-3.

[27] Y.-X. Li, J. Rinzel, Equations for $InsP_3$ receptor-mediated Ca^{2+} oscillations derived from a detailed kinetic model: a Hodgkin-Huxley-like formalism, J Theor Biol 166 (1994) 461–73.

[28] G. Dupont, C. Erneux, Simulations of the effects of inositol 1,4,5-trisphosphate 3-kinase and 5-phosphatase activities on Ca^{2+} oscillations, Cell Calcium 22 (5) (1997) 321–31.

[29] J. K. Foskett, C. White, K.-H. Cheung, D.-O. D. Mak, Inositol trisphosphate receptor Ca^{2+} release channels, Physiol Rev 87 (2) (2007) 593–658.

[30] L. E. Wagner, D. I. Yule, Differential regulation of the $InsP_3$ receptor type-1 and -2 single channel properties by $InsP_3$, Ca^{2+} and ATP, J Physiol 590 (14) (2012) 3245–59.

[31] I. Siekmann, L. E. Wagner, D. Yule, E. J. Crampin, J. Sneyd, A kinetic model for type I and II IP_3R accounting for mode changes, Biophys J 103 (4) (2012) 658–68.

[32] P. Cao, X. Tan, G. Donovan, M. J. Sanderson, J. Sneyd, A deterministic model predicts the properties of stochastic calcium oscillations in airway smooth muscle cells, PLoS Comput Biol 10 (8) (2014) e1003783. doi:10.1371/journal.pcbi.1003783.

[33] D. D. Friel, $[Ca^{2+}]_i$ oscillations in sympathetic neurons: an experimental test of a theoretical model, Biophys J 68 (5) (1995) 1752–66.

[34] N. L. Allbritton, T. Meyer, L. Stryer, Range of messenger action of calcium ion and inositol 1,4,5-trisphosphate, Science 258 (1992) 1812–1815.

[35] G. W. De Young, J. Keizer, A single-pool inositol 1,4,5-trisphosphate-receptor-based model for agonist-stimulated oscillations in Ca^{2+} concentration, Proc Natl Acad Sci USA 89 (20) (1992) 9895–9.

[36] A. Politi, L. D. Gaspers, A. P. Thomas, T. Höfer, Models of IP_3 and Ca^{2+} oscillations: frequency encoding and identification of underlying feedbacks, Biophys J 90 (9) (2006) 3120–33.

[37] A. Tanimura, T. Morita, A. Nezu, A. Shitara, N. Hashimoto, Y. Tojyo, Use of fluorescence resonance energy transfer-based biosensors for the quantitative analysis of inositol 1,4,5-trisphosphate dynamics in calcium oscillations, J Biol Chem 284 (13) (2009) 8910–7. doi:10.1074/jbc.M805865200.

[38] L. Palk, A mathematical study of the role of calcium in the regulation of saliva secretion, Ph.D. thesis, University of Auckland (2012).